Mining, Metallurgy & Exploration (2021) 38:539–547
https://doi.org/10.1007/s42461-020-00349-9

Thermal Runaway Pressures of Iron Phosphate Lithium-Ion Cells as a Function of Free Space Within Sealed Enclosures

Thomas H. Dubaniewicz[1] · Isaac Zlochower[1] · Teresa Barone[1] · Richard Thomas[1] · Liming Yuan[1]

Received: 3 June 2020 / Accepted: 27 October 2020 / Published online: 6 November 2020

Abstract
Mining vehicle manufacturers are developing lithium-ion (Li-ion) battery electric vehicles as an alternative to diesel-powered vehicles. In gassy underground mines, explosion-proof (XP) enclosures are commonly used to enclose electrical ignition sources to prevent propagation of an internal methane (CH_4) air explosion to a surrounding explosive atmosphere. Li-ion batteries can create pressurized explosions within sealed enclosures due to thermal runaway (TR). Researchers at the National Institute for Occupational Safety and Health (NIOSH) measured TR pressures of lithium iron phosphate (LFP) cells as a function of free space within sealed enclosures and observed an inverse power relationship. A well-confined cell produced 294 bar (4260 psia) of pressure during a TR, far exceeding minimum pressure containment specifications for conventional XP enclosures. Results indicate that adding enough free space surrounding LFP cells can reduce TR pressures to levels below that expected for CH_4-air ignitions. Measured TR temperatures were below the minimum autoignition temperature of CH_4-air.

Keywords Batteries · Lithium-ion · Thermal runaway · Explosion proof · Flameproof · Battery electric vehicle

1 Introduction

Mining vehicle manufacturers are developing battery electric vehicles (BEVs) powered by lithium-ion (Li-ion) batteries as an alternative to diesel-powered vehicles. Given the relatively high energy density of Li-ion batteries, they are currently the most common battery of choice for new BEV applications [1]. Large-format batteries of hundreds of volts sourcing hundreds of amperes are constructed from series and parallel connections of smaller cells or modules. An international survey of mining operators [2] identified health, economic, and environmental factors favoring the electrification of mining operations. Harrop [3] forecasts that the electrification and automation of mining vehicles will be a $15 billion market by 2028. Diesel emissions, from diesel-powered vehicles in mining, pose a health hazard and have been classified as "Group 1: carcinogenic to humans" by the World Health Organization [4]. The benefits of employing BEVs are arguably greater for underground mining than any other industry [1]. Approximately 15,000 underground coal miners and 13,000 underground metal/non-metal miners in the USA are exposed to aerosols and gases emitted by diesel engines, and exposure of underground miners to diesel aerosols is the highest among workers in all occupations [5].

The potential use of Li-ion BEVs in gassy underground mines poses unique explosion hazards. Explosive methane (CH_4) gas may be liberated in underground coal, salt, trona, potash, limestone, copper, and uranium mines [6]. Li-ion battery thermal runaway (TR) is a potential ignition source for CH_4-air atmospheres [7–9]. Furthermore, the TR process produces high temperatures and significant amounts of gas [10] that can result in excessive pressure. Dubaniewicz and Ducarme [7, 9] found that TR pressures on the order of 103 bar (1500 psi) or greater had been observed by several laboratories. The highest pressures were measured in enclosures providing little free space around the battery.

A widely cited National Highway Traffic Safety Administration (NHTSA) report [11] concluded that the propensity and severity of fires and explosions from the accidental ignition of flammable electrolytic solvents used in Li-ion battery systems are anticipated to be somewhat comparable with or perhaps slightly less than those for gasoline or diesel vehicular fuels. Furthermore, the overall consequences from Li-ion batteries are expected to be less because of the much

✉ Thomas H. Dubaniewicz
Tcd5@cdc.gov

[1] Pittsburgh Mining Research Division (PMRD), The National Institute for Occupational Safety and Health (NIOSH), Pittsburgh, PA, USA

smaller amounts of flammable solvent released and burning in a catastrophic failure situation. Cell-casing rupture and release of projectiles (if pressure relief devices are not present or if they fail) was identified as a potential primary hazard associated with TR-induced heat and pressure. The report's conclusions for explosion severity were based on a comparison of vehicular fuel and lithium electrolytic solvent flammability characteristics, including maximum blast overpressures in the range of 7.5 to 7.9 atm (110 to 116 psi). The cited flammability characteristics were for fuel-air mixtures. Henrikson et al. [12] reported similar overpressure values for Li-ion battery electrolyte solvent-air mixtures. However, Li-ion cells undergoing TR and without involvement of atmospheric oxygen can produce pressures exceeding 7.9 atm by over an order of magnitude, as discussed above in the review of [7] and [9].

Explosion-proof (XP) enclosures are commonly used in potentially explosive atmospheres in mines to enclose electrical ignition sources to prevent propagation of an internal CH_4-air explosion to a surrounding CH_4-air contaminated atmosphere. The Mine Safety and Health Administration (MSHA) defines an explosion-proof enclosure as an enclosure that complies with the applicable design requirements of 30 CFR 18 and is so constructed that it will withstand internal explosions of methane-air mixtures: (1) without damage to or excessive distortion of its walls or cover(s) and (2) without ignition of surrounding methane-air mixtures or discharge of flame from inside to outside the enclosure [13]. Among other design requirements, enclosures must be designed to withstand a minimum pressure of at least 150 psig (10.3 bar) without leakage through any welds or castings, rupture of any part that affects explosion-proof integrity, clearances exceeding those permitted under existing requirements along flame-arresting paths, or permanent distortion exceeding 0.040-inch per linear foot. External surfaces of enclosures shall not exceed 150 °C (302 °F). For required explosion testing [14], if any pressure peak exceeds 125 psig (8.62 bar), the manufacturer must either make constructional changes that will result in a reduction of pressure to 125 psig or less or conduct static pressure tests of the enclosure, with the enclosure withstanding a static pressure of twice the highest value recorded in any previous tests. A maximum pressure of 104 psig (7.17 bar) can be realized from a CH_4-air ignition in a closed vessel without the effects of pressure piling [15]. Pressures in excess of 104 psig may result from pressure piling or turbulence. These MSHA requirements and test procedures pertain to ignition of CH_4-air mixtures within the enclosure. There are no test procedures for assessing pressures from Li-ion battery thermal runaway.

Researchers at the National Institute for Occupational Safety and Health (NIOSH), Pittsburgh Mining Research Division (PMRD), recently began a study of approaches to mitigate fire and explosion hazards of Li-ion batteries used for mining equipment. In this work, researchers characterized TR pressures of lithium iron phosphate (LFP) cells as a function of enclosure free space using various sizes of sealed enclosures. Iron phosphate cathode is one of several Li-ion chemistries used for mining BEVs [1]. Enclosure-confined cells were heated in an accelerating rate calorimeter (ARC) to attain TR, simulating excessive temperatures within XP enclosures due to potential internal CH_4-air ignition, electrical fault within a large-format battery, or fault within Li-ion cells susceptible to TR from internal short circuit. Results indicate that enough free space surrounding the LFP cells alone (without CH_4-air present) can reduce TR pressures to below the 125-psig threshold per the MSHA requirement [14].

2 Methods

The LFP cells selected for this study were cylindrical spiral-wound types 18650 and 26650 from the same manufacturer. The rated capacities were 1.5 Ah and 3.8 Ah, respectively. The cells were conditioned with three charge-discharge cycles followed by a charge to 100% state of charge. An Arbin multi-channel potentiostat/galvanostat (MSTAT) cycled the cells using cell-manufacturer-specified parameters. Measured discharge capacities were at least 97% of rated capacity.

Researchers analyzed the composition of an LFP cell to identify the electrolyte solvent and to confirm the composition of other components. The morphology and elemental composition of the anode, cathode, and separator of a type 26650 cell were analyzed by scanning electron microscopy (SEM) (Model S-4800, Hitachi, Tokyo, Japan) and energy-dispersive x-ray spectroscopy (EDS) (Bruker Quantax, Madison, Wisconsin), respectively. Samples were mounted on 25-mm aluminum posts using conductive carbon tape. The separator was sputter-coated with a conductive layer of gold and palladium for 2 min to improve image clarity. Images were acquired at 5 and 20 kV and 10^3–5×10^4 magnification, and elemental compositions were analyzed at 20 kV.

In addition to elemental analysis, the separator was analyzed by transmission Fourier transform infrared spectrometry (FTIR) (model Alpha from Bruker, Billerica, MA) to examine for functional groups associated with the separator film and adsorbed electrolyte solvent. Solvent-associated functional groups were studied by comparing transmission FTIR spectra for the slightly moist and nearly dry separator samples. For sample preparation, part of the separator was unwrapped from a coiled battery cell, a 25-mm piece was cut and placed in a film holder, and a 6-mm section of the center was analyzed. Spectra were collected in transmission mode at 2-cm^{-1} resolution by averaging 40 scans and were saved from 399.5–3998.5 cm^{-1}. The preparation and analysis were completed within 2 minutes and were repeated three times for different

sections of the separator. Subsequently, the separator samples were heated to 110 °C in a drying oven and were re-analyzed. Spectra acquired before and after heating were subtracted using OPUS software (Bruker, Billerica, MA) to evaluate solvent-associated peaks.

Researchers used a Thermal Hazard Technology (THT) ARC system comprising an EV+ and standard ARC to conduct TR pressure tests. Each LFP cell was sealed within a canister placed within the ARC. The ARC temperature was raised to a constant value to provide steady-state heating until the cell reached TR. The heaters shut off after TR detection. The standard ARC was used for one test with an 18650 cell within a form-fitting canister. The EV+ ARC was used for all other TR pressure tests. ARC instrumentation included a 0-207 bar (3,000 psi) pressure sensor, voltage inputs, and type N thermocouples. A THT ARC enhanced system (ARCes) control and data acquisition software recorded sensor data. The data was imported into Microsoft Excel for plotting and trend calculations.

Temperature measurements included cell temperature, canister internal gas temperature, and canister exterior surface temperature. The cell thermocouple was taped to the metallic surface of the cell about mid-length with fiber tape. The gas thermocouple was inserted into free space within the canister, and the canister thermocouple was taped to the canister exterior.

Various sizes of canisters provided different amounts of free space around the LFP cells (Fig. 1). Table 1 lists combinations of cell types and canisters used for pressure measurements. The cell volume was calculated from the nominal diameter and height. A 19.6-mL stainless steel canister with a short section of steel tubing supplied by the THT ARC system provided a form fit to the 18650 cell. The free space volume for this canister is the calculated internal volume of steel tubing connecting the canister to a pressure sensor fitting outside of the standard ARC. The other canisters were constructed in-house from steel pipe nipples with caps screwed onto both ends. The pipe nipple canisters were used in the EV+ ARC exclusively. Their internal volumes were measured by filling them with water. The 2795-mL nipple canister is schedule 40, and the other nipple canisters are schedule 80. The caps were drilled and tapped to accept compression fittings for instrumentation connections. Canister seal integrity was checked prior to ARC tests using a manometer and a pneumatic hand pump.

3 Results

3.1 Cell Composition

The LFP cells were described by the manufacturer as containing a lithium ferro-phosphate ($LiFePO_4$) cathode. This was verified by SEM/EDS elemental x-ray analysis, which showed a collection of irregular particles ≤ 1 μm in size that had strong iron (Fe), phosphorus (P), and oxygen (O) x-ray peaks. Some x-ray energy spectra even showed a weak Li peak. There was also a weak aluminum (Al) peak which, presumably, arose from the Al foil substrate, and a weak carbon (C) peak, ostensibly, from carbon black added to provide better electron conductivity to the cathode.

The anode showed larger (≈ 10 μm) flat particles that had a predominant C peak. The shape and high C content of the particles were consistent with a graphite-based anode. There were also weak peaks of P, fluorine (F), and, possibly Li (very weak) which could be attributed to an absorbed $LiPF_6$ electrolyte. There was also a very weak copper (Cu) peak attributed to the Cu foil substrate of the anode layer.

The separator film was examined with the SEM/EDS instrument and by FTIR transmission spectroscopy. The SEM images showed a coating of ≤ 1-μm irregular particles that produced strong Al and O peaks consistent with an aluminum oxide (Al_2O_3) coating. There was also a weak C peak attributed to the porous organic film at the core of the separator layer. FTIR absorption spectra of the wet (cell liquid) and dried samples of separator material were consistent with the presence of ethylene carbonate in the solvent and a polyethylene film. The alumina coating is largely transparent in the IR range examined but appeared to show its presence near the low energy end of the spectrum (> 900 cm^{-1}).

Table 1 Cell and canister volumes

Cell type	Cell vol. (mL)	Canister internal vol. (mL)	Free space (mL)	Free space/cell vol.
18650	16.54	19.6	3.06	0.185
26650	34.51	220	185	5.36
26650	34.51	370	335	9.71
18650	16.54	220	203	12.3
26650	34.51	735	700	20.3
26650	34.51	1295	1260	36.5
18650	16.54	735	718	43.4
26650	34.51	2795	2760	80

Fig. 1 Canisters provided varying amounts of free space around enclosed Li-ion cells

3.2 Gas Generation

Gas generation from the cell occurs as the cell surface is heated to a critical temperature, wherein heat and gas generation rates enter into a positive feedback loop and increase exponentially, reaching a TR. For an LFP cell, this critical temperature is about 200 °C (depending on the rate of external heating). Gas generation into the confining vessel (canister) starts at a lower temperature as some of the gas pressure in the cell is relieved (cell venting). The major pressure rise, however, occurs sharply at the runaway temperature when the cell pressure and rate of pressure rise (dp/dt) are sufficient to release much of the gas suddenly. The associated pressure rise in the canister is due to its sudden gas temperature rise as well as the moles of gas released into the vessel. Those gas moles are calculated as a function of heating time from the gas temperature and pressure data, using the free volume of the vessel and the ideal gas law. The resulting plot is shown in Fig. 2 for the 26650 LFP cell in a 2795-cm^3 vessel (canister) volume. The plot of moles gas released into the canister versus heating time is seen to be very similar to the corresponding pressure record in Fig. 3. The gas moles liberated by the cell reach a peak at the TR and remain reasonably steady up to the point where cooling causes the less volatile species to start condensing. Thus, the maximum value of the moles of gas produced was 0.290 mol just after the TR. It can be assumed that the minor gas increase noted after the TR is due to reaction of the hot gas released with the air in the canister. The final mole of gas at the end of the ARC run at 50 °C is, however, 0.211 mol. This 27.3% reduction in gas is attributed to the above condensation phenomenon. A small canister leak at elevated temperature and pressure is also possible. The gradual reduction in pressure over several hours while the canister cooled indicates that any potential leakage was small. Converting to ambient temperature and pressure (22 °C and 1.00 bar) gives an equivalent volume of 7.11 L from the peak gas production and 5.18 L from the final run conditions. Considering that the volume of air within the canister at initial room conditions was approximately 2.76 L, the amount of gas generated by the cell converted to ambient temperature and pressure was approximately 4.35 L.

3.3 Thermal Runaway Pressures

Figures 3 and 4 show time plots for two ARC tests using the largest (Fig. 3) and smallest (Fig. 4) canisters. Pressure measurements were absolute. Figure 3 shows results for a 26650 LFP cell within the 2795-mL canister. The cell temperature

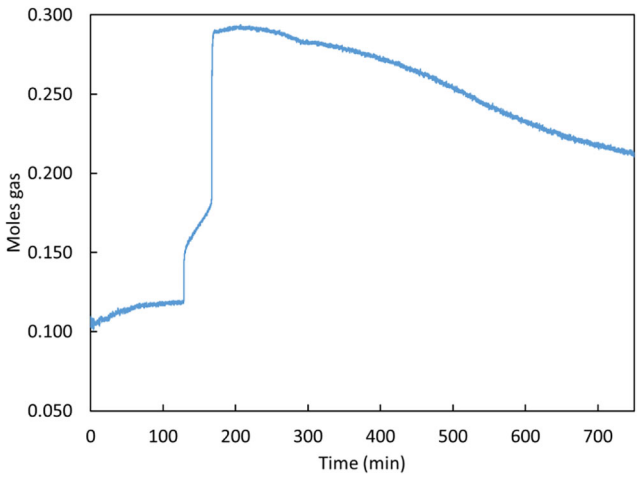

Fig. 2 The moles of gas liberated into the 2795 canister from a 26650 LFP cell as a function of heating time for the ARC ramp test shown in Fig. 3

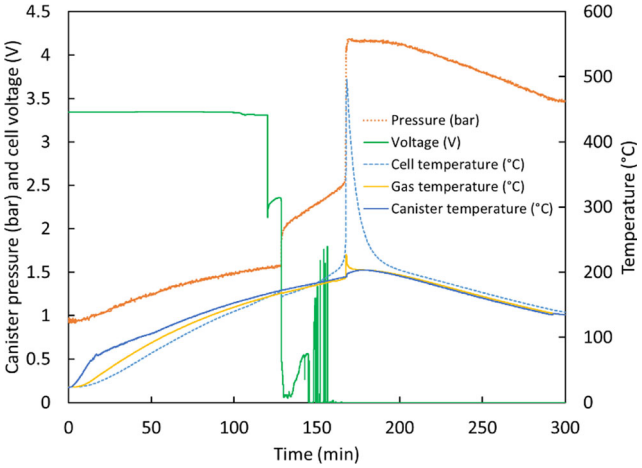

Fig. 3 Time plots of canister absolute pressure, cell voltage, and temperatures for an ARC ramp test of a 26650 LFP cell within a 2795-mL canister.

reached a maximum of 496 °C, measured by a thermocouple taped to the cell. The cell temperature at the onset of venting was approximately 170 °C. Canister pressure increased with temperature prior to cell venting. Cell voltage dropout occurred before cell venting. Venting produced an additional increase in canister pressure accompanied by a brief decrease in cell temperature. TR occurred after venting, indicated by a rapid increase in both pressure and temperature. The pressure peaked at 4.19 bar before gradually decreasing as the canister cooled. In contrast, a much higher pressure of 294 bar was measured in the 19.6-mL canister containing an 18650 LFP cell under similar heating conditions (Fig. 4). The 19.6-mL canister was ruptured (Fig. 5) after reaching 294 bar, indicated by the abrupt decrease in pressure in Fig. 4. The thermocouple was taped to the canister exterior, and cell voltage was not recorded due to space limitations within the canister.

Table 2 lists summary data of TR pressures for the LFP cells confined within the different canisters. Three tests were conducted with each cell and canister combination, except for

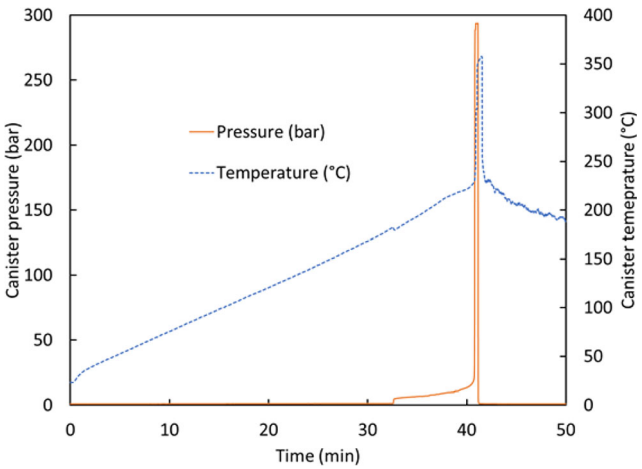

Fig. 4 Time plots of canister absolute pressure and temperature for an ARC ramp test of an 18650 LFP cell within a 19.6-mL canister

Fig. 5 The ruptured 19.6-mL canister next to an undamaged canister

the 19.6-mL canister which ruptured. Figure 6 plots TR pressure versus the ratio of free space to cell volume. Small variations in test conditions have a greater impact on measured pressure variability nearer to the vertical portion of the curve in Fig. 6. The 19.6-mL canister result is not shown in Fig. 6 but is included in the trend curve calculations. Two trend curves are shown. The lower curve (TR pressure) includes all data, and the top curve (peak TR pressure) includes only the highest pressure per cell-canister combination. The trend curves for both sets of data fit an inverse power relationship ($R^2 > 0.97$). The amount of free space surrounding the cell may be used to predict TR pressure.

The 294-bar result in Table 2 is above the calibrated range and below the damage threshold of the pressure sensor per the sensor manufacturer. Figure 7 shows a plot of natural log (Ln) transformed data, including the 294-bar result corresponding to the negative independent value. The data produced a good ($R^2 > 0.97$) straight line fit as expected for an Ln-transformed power function. The 294-bar result is slightly below the trend line, indicating a reasonable fit with the data. The trend suggests that slightly higher pressures than 294 bar may be expected under similar test conditions.

3.4 Temperatures

Cell, gas, and canister temperatures were recorded while the cells were heated to TR such as for the test shown in Fig 3. Cell heating from internal exothermic processes (including chemical reactions and internal short circuit) increased after venting as cell temperature crossed over to exceed the canister exterior surface temperature. Peak cell and gas temperatures resulted from external heating and heating from cell internal exothermic processes. Temperature summary data for tests in Table 2 (not including parallel-cell tests described in the next

Table 2 Thermal runaway absolute pressure for LFP cells within canisters

18650		26650	
Free space/cell vol.	TR pressure bar	Free space/cell vol.	TR pressure bar
0.185	294	5.36	36.5
12.3	16.6	5.36	38.9
12.3	16.8	5.36	31.4
12.3	17	9.71	26.5
43.4	6.19	9.71	20.7
43.4	6.1	9.71	20
43.4	6.15	20.3	16.5
		20.3	11
		20.3	15.5
		36.5	6.68
		36.5	11
		36.5	7.23
		80	4.28
		80	4.52
		80	4.19

section) are shown as box and whisker plots in Figs. 8 and 9. The temperature at venting onset is the temperature at which initial venting became apparent from dp/dt data. The difference between peak and venting onset temperatures provides an approximation of temperature rise due to TR.

3.5 Parallel Cells

Parallel-connected cells may feed current to a failing cell, possibly enhancing energy release. Three EV+ ARC tests were conducted with two fully charged 26650 LFP cells connected in parallel to a fully charged 26650 LFP cell that was sealed within the 735-mL canister (20.3 free space/cell vol.) placed within the EV+. The two parallel cells were located outside of the ARC and connected to the confined cell using 10-gauge wire routed through a current sensor. The confined cell was heated by the EV+ until TR occurred. Time plots for the parallel-cell ARC test that produced the highest discharge current (76 A) and canister pressure (17.6 bar) are shown in Fig. 10. The cell contents were ejected from the cell for this test. The discharge current may have been shorted through the active material or to the case of the failed cell. Summary data for the parallel-cell ARC tests are listed in Table 3. Peak cell and gas temperatures fell within the range of temperatures for the single-cell ARC tests (Fig. 9). For test #2 in Table 3, the cell under test received current beginning at venting onset but disconnected from the parallel cells at the peak of TR. The parallel cells only partially discharged to 3.3 V for test #2. Peak pressures for these three tests averaged 14.8 bar. In comparison, the peak pressures for the 20.3 free space/cell vol. tests listed in Table 2 ranged from 11 to 16.5 bar, averaging 14.3 bar. Discharge from the parallel cells produced an average pressure increase of 0.5 bar compared with the single-cell tests. The energetic nature of TR makes it difficult to maintain connection to external circuits.

4 Discussion

Conventional MSHA-approved XP enclosures are designed such that internal ignitions will produce pressures of 125 psig (8.62 bar) or less [14]. If a manufacturer cannot make constructional changes to reduce ignition pressure to the 125-psig threshold, the enclosure must be designed to withstand a static pressure of twice the highest value observed during ignition tests. Using the peak TR pressure curve fit equation shown in Fig. 6 and accounting for gauge versus absolute pressure measurements, approximately 34 times the LFP cell volume of

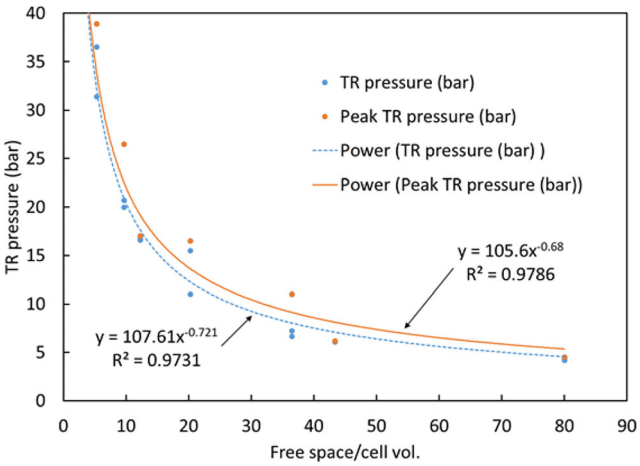

Fig. 6 A plot of an inverse power relationship between thermal runaway pressure and the ratio of free space-to-cell volume

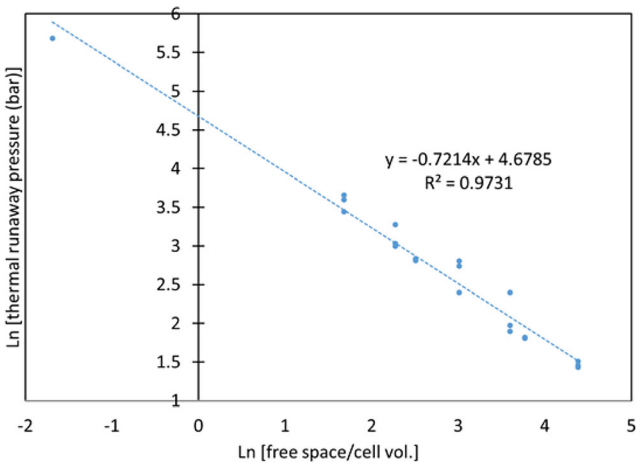

Fig. 7 A linear relationship between Ln-transformed TR pressure and free space/cell volume.

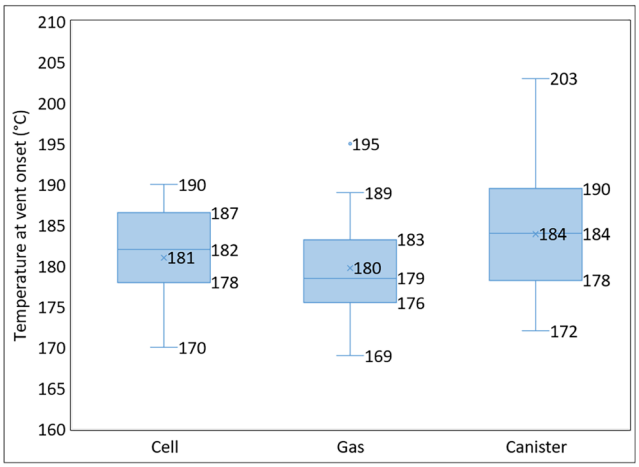

Fig. 8 Box and whisker plots summarizing cell, gas, and canister temperatures at venting onset.

free space would be needed to meet the 125-psig threshold. This approximation is for cells of similar construction and chemistry to the LFP cells studied here.

Criteria for evaluation and testing of MSHA-approved XP enclosures may need to consider the cumulative internal pressure resulting from a simultaneous CH_4-air ignition and the pressure from a TR event from an LFP cell.

Large-format batteries are constructed from series and parallel connections of smaller cells or modules. A large-format battery may be designed to contain TR to a limited number of cells or modules to prevent a cascading TR throughout the battery. The amount of free space needed to limit TR pressure in a sealed enclosure for such a battery could be based on accounting for a foreseeable number of independent failures resulting in TR for a limited number of cells or modules. Multiple cells or modules prone to ignition by a common source should be considered as a single independent failure. Such an approach may favor using larger numbers of small cells or modules over fewer numbers of large cells or modules to reduce free space needs.

Table 3 Summary of peak measurements for parallel-cell ARC tests using the 735-mL canister

Test	1	2	3
Discharge current (A)	76	43	46
Pressure (bar)	17.6	13.2	13.7
Cell temperature (°C)	410	347	288
Gas temperature (°C)	318	213	242

Properly designed and maintained flame arrestors can provide pressure relief of ignitions within sealed enclosures while preventing ignition of a surrounding explosive atmosphere. The knowledge of Li-ion TR pressure may indicate where the use of a properly designed flame arrestor is warranted and an upper bound of the amount of pressure due to Li-ion TR that the flame arrestor must accommodate.

The LFP cells were tested at a full state of charge. The severity of the thermal runaway increases with an increasing state of charge [16]. Results of this study should not be considered conservative for cells at an excessive state of charge due to overcharge.

Where other chemistry and construction features are similar, metal oxide cathode Li-ion cells may fail more energetically than LFP cells. Results of this study should not be considered conservative for such metal oxide cathode Li-ion cells.

Kuchta [17] reviewed CH_4 ignition temperatures by heated vessels, surfaces, and jets of hot gases. Minimum autoignition temperature (AIT) refers to the lowest temperature for the ignition of a flammable substance within a heated vessel. An experimentally observed AIT for CH_4-air is 600 °C [18]. Heated wire, rod, or tube ignition temperatures are normally much higher than heated vessel ignition temperatures [17].

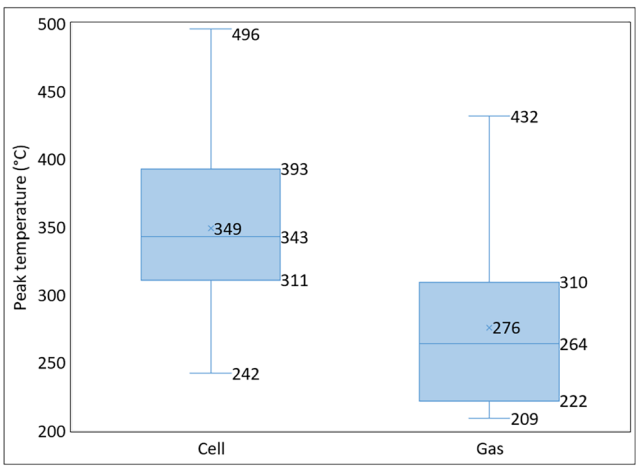

Fig. 9 Box and whisker plots summarizing peak cell and gas temperatures

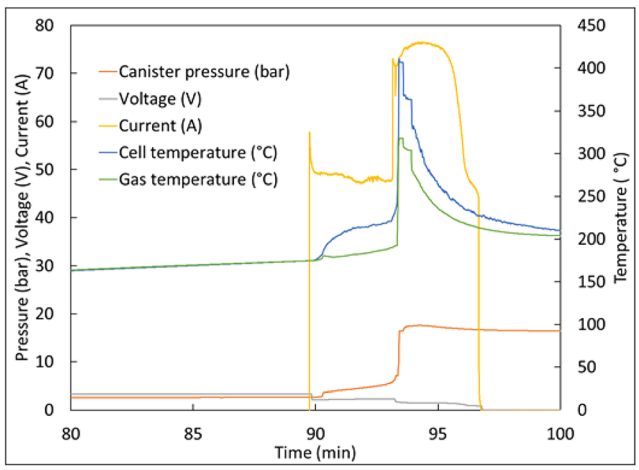

Fig. 10 Time plots of pressure, voltage, current, and temperatures for a parallel-cell ARC test

Kuchta [17] reported CH_4 ignition by an air-jet heated to 1040 °C. Hot gas ignition temperatures are useful in evaluating the ignition hazard of possible hot gases evolved from flame arrestors or explosion-proof seals.

Even with external heating to initiate TR, the peak LFP cell and gas temperatures were below the 600 °C AIT or 1040 °C heated air-jet ignition temperature for CH_4-air. The LFP TR gases or cell surface of the individual cells may not be hot enough to ignite CH_4-air mixtures. In previous research [7–9], internally shorted LFP cells did not ignite CH_4-air mixtures, while some other internally shorted Li-ion cell chemistries did ignite CH_4-air mixtures. Along with ambient CH_4, vented LFP cell gases mixed with air may form flammable gas-air mixtures, which may be ignited by a sufficiently strong ignition source such as an electrical fault of a large format battery.

Kuchta [17] lists layer and cloud ignition temperatures for several types of coal dust. Listed coal dust layer ignition temperatures range from 160 to 220 °C depending on the coal source. Layers of coal dust may readily accumulate on enclosure surfaces at coal mining or processing operations, and MSHA requires that external surfaces of explosion-proof enclosures shall not exceed 150 °C (302 °F) [13]. Listed coal dust cloud ignition temperatures range from 440 to 640 °C [17]. Measured LFP TR gas temperatures fall within this range. The external heating by the ARC to initiate TR should be taken into consideration for an ignition hazard assessment if there is a possibility of LFP TR gas exposure to coal dust clouds outside of the enclosure (e.g., through a flame arresting vent).

5 Conclusions

NIOSH PMRD researchers are developing workplace solutions to reduce the explosion risks of Li-ion batteries in mining equipment.

The gas liberated by the ruptured cell during thermal runaway as well as its characteristic temperature rise is responsible for the pressure developed in the containment vessel, as implied by Fig. 2.

An inverse power relationship was observed between thermal runaway pressure and the amount of free space surrounding selected iron phosphate Li-ion cells within sealed enclosures. The amount of free space surrounding the cell may be used to predict thermal runaway pressure. A thermal runaway pressure of 294 bar (4260 psia) was observed for a well-confined cell. A curve fit to the data indicates that approximately 34 times the cell volume of free space would be needed to produce an 8.62 bar (125 psig) thermal runaway pressure. Increasing the amount of free space within sealed enclosures containing these iron phosphate cells can reduce thermal runaway pressures.

Even with external heating to initiate thermal runaway in the iron phosphate cells, observed peak cell and gas temperatures were below the 600 °C autoignition temperature and 1040 °C heated air-jet ignition temperature for methane-air. This suggests that the thermal runaway gases or cell surface of the individual cells studied here may not be hot enough to ignite methane-air mixtures. Along with ambient methane, vented iron phosphate Li-ion cell gases mixed with air may form flammable gas-air mixtures, which may be ignited by a sufficiently strong ignition source such as an electrical fault of a large format battery.

Acknowledgments The authors wish to thank John Soles of the Pittsburgh Mining Research Division for conducting ARC tests.

Compliance with ethical standards

Disclaimer The findings and conclusions in this report are those of the authors and do not necessarily represent the official position of the National Institute for Occupational Safety and Health, Centers for Disease Control and Prevention. Mention of any company or product does not constitute endorsement by NIOSH.

Conflict of Interest The authors declare that they have no conflict of interest.

References

1. GMSG (2017) Recommended practices for battery electric vehicles in underground mining. Global Mining Standards and Guidelines. 20160726_UG_Mining_BEV-GMSG-WG-v01-r01. Ormstown, QC, CA.
2. Mitchell, P (2019) Will electrification spark the next wave of mining innovation? EYGM Limited. EYG no. 003211-19Gbl. 16 pp. Retrieved August 2019 from https://www.ey.com/en_us/mining-metals/will-electrification-spark-the-next-wave-of-mining-innovation.
3. Harrop P (2018) Electric vehicles and autonomous vehicles in mining 2018-2028: technologies, challenges, benefits, markets, forecasts, key players and opportunities. IDTechEX, Boston, p 280
4. International Agency for Research on Cancer (2012) IARC: diesel engine exhaust carcinogenic [Press Release No. 213]. World Health Organization. Retrieved August 2019 from https://www.iarc.fr/en/media-centre/pr/2012/pdfs/pr213_E.pdf.
5. NIOSH (2017) Mining project: advance strategies for controlling exposures to diesel aerosols. U.S. Department of Health and Human Services, Centers for Disease Control and Prevention, National Institute for Occupational Safety and Health, Cincinnati Retrieved September 2019 from https://www.cdc.gov/niosh/mining/researchprogram/projects/project_DieselAerosols.html.
6. NIOSH (2006) Handbook for methane control in mining. By Kissel FN. Pittsburgh, PA: U.S. Department of Health and Human Services, Centers for Disease Control and Prevention, National Institute for Occupational Safety and Health, DHHS (NIOSH) Publication No. 2006-127, Information Circular 9486, 2006 Jun: 1-184. Retrieved August 2019 from https://www.cdc.gov/niosh/mining/UserFiles/works/pdfs/2006-127.pdf.
7. Dubaniewicz TH, DuCarme JP (2013) Are lithium-ion cells intrinsically safe? IEEE Trans Ind Appl 49(6):2451–2460 Retrieved

August 2019 from http://www.cdc.gov/niosh/mining/Works/coversheet1864.html.
8. Dubaniewicz TH, DuCarme JP (2014) Further study of the intrinsic safety of internally shorted lithium and lithium-ion cells within methane-air. J Loss Prev Process Ind 32:165–173 Retrieved August 2019 from http://www.ncbi.nlm.nih.gov/pmc/articles/PMC4485987/.
9. Dubaniewicz TH, DuCarme JP (2016) Internal short circuit and accelerated rate calorimetry tests of lithium-ion cells: considerations for methane-air intrinsic safety and explosion proof/flameproof protection methods. J Loss Prev Process Ind 43:575–584 Retrieved August 2019 from https://www.ncbi.nlm.nih.gov/pmc/articles/PMC5040472/.
10. Roth EP, Crafts CC, Doughty DH, McBreen J (2004) Advanced technology development program for lithium-ion batteries: thermal abuse performance of 18650 Li-ion cells. Sandia Nat. Lab., Albuquerque Rep. SAND2004-0584, Retrieved August 2019 from https://pdfs.semanticscholar.org/7c66/2ecf8d3c4830c84283f225504e5b2f454ba8.pdf.
11. Stephens D, Shawcross P, Stout G, Sullivan E, Saunders J, Risser S, Sayre J (2017) Lithium-ion battery safety issues for electric and plug-in hybrid vehicles (Report No. DOT HS 812 418). National Highway Traffic Safety Administration, Washington, DC Retrieved August 2019 from https://www.nhtsa.gov/sites/nhtsa.dot.gov/files/documents/12848-lithiumionsafetyhybrids_101217-v3-tag.pdf.
12. Henriksen M, Vaagsaether K, Lundberg J, Forseth S, Bjerketvedt D (2019) Explosion characteristics for Li-ion battery electrolytes at elevated temperatures. J Hazard Mater 371:1–7
13. 30 CFR (2018) Code of federal regulations, mineral resources, parts 1 to 199. U.S. Department of Labor, Mine Safety and Health Administration, Arlington Retrieved August 2019 from https://arlweb.msha.gov/regs/30cfr/.
14. MSHA (2005) Requirements for explosion testing per 30 CFR, 18.62, ASTP 2137. U.S. Department of Labor, Mine Safety and Health Administration, Arlington, VA, USA. Retrieved August 2019 from https://arlweb.msha.gov/TECHSUPP/ACC/StandardTestProcs/ASTP2137.pdf.
15. Boring RC, Beasley WC, Bedway BF, Murtaugh SM, Warnock WS (2005) Report of investigation - part 6 equivalency review and comparison: MSHA and IEC explosion-proof enclosure standards. U.S. Department of Labor, Mine Safety and Health Administration, Directorate of Technical Support, Approval and Certification Center, Triadelphia
16. Golubkov AW, Scheikl S, Planteu R, Voitic G, Wiltsche H, Stangl C, Fauler G, Thaler A, Hacker V (2015) Thermal runaway of commercial 18650 Li-ion batteries with LFP and NCA cathodes – impact of state of charge and overcharge. RSC Adv 5:57171–57186
17. Kuchta JM (1985) Investigation of fire and explosion accidents in the chemical, mining, and fuel-related industries—a manual, bulletin 680. U.S. Department of the Interior, Bureau of Mines, Pittsburgh
18. Robinson C, Smith DB (1984) The auto-ignition temperature of methane. J Hazard Mater 8(3):199–203